International Journal of Medical Toxicology & Legal Medicine Volume 27, No. 4, 2024
e-ISSN: 0974-4614
p-ISSN: 0972-0448

Assessment of lung cancer, its treatment with radiotherapy, and its Dose Calculation

Tareg Mohammed H Al Mansour[1], Hassan Saleh M Al Khamsin[1], Ibrahim Ali M Alsulaiman[1], Mohammed Husaain A Alyami[2], Mohammed Mahdi Hadi Alajmi[3], Abdullah Hussain Salem Alyami[4], Masaud Mohammed Alyami[5], Saleh Rajeh Alyami[6]

[1]New Najran General Hospital, Medical Physicist.
[2]New Najran General Hospital, Radiographer Technologist.
[3]Senior Specialist of Radiological Technology, King Khalid Hospital in Najran.
[4]Diagnostic Radiology, New Najran General Hospital.
[5]Najran Cluster, Radiology Specialist.
[6]Radiology Technologist, Abqaiq General Hospital.

Received: 10.08.2024 Revised: 18.09.2024 Accepted: 22.10.2024

ABSTRACT

Background: Lung cancer ranks among the top causes of illness and death globally, highlighting the need for effective treatment approaches. This study aimed to explore the use of radiotherapy in lung cancer treatment, with a focus on dose adjustments for lung inhomogeneity and density variations.

Materials and Methods: The study's methodology was divided into two stages. In the first stage, a computerized treatment planning system was used to set up configurations and procedures. After refining the initial data within this system, the second phase involved gathering experimental results using an ionization chamber as a standard. Treatment planning in this study required advanced techniques for targeting lung cancer, considering shifts in dose variance as lung density fluctuates. The Collapsed Cone Convolution Superposition (CCCS) model was employed to evaluate lung dose calculations in terms of lung density, treatment geometry, and dosage comparisons.

Results: Findings from the study suggest that homogeneous dose calculations from CCCS align closely—within 1%—with those from the adaptive convolution (AC) method. This indicates that AC, with its faster processing capability, may serve as a viable alternative to CCCS.

Conclusion: Dose absorption calculations derived from the treatment planning system (TPS) based on the CCCS algorithm yield highly accurate results. This accuracy is supported by Monte Carlo calculations, which are effective in modeling heterogeneous media and low-density materials, such as lung tissue.

Keywords: lung cancer, small cell lung cancer, non-small cell lung cancer, radiotherapy, Dose Calculation, heterogeneous media, low-density materials.

1. INTRODUCTION

An aberrant development of cells that group together in the lungs and impact the surrounding healthy lung tissues is what causes lung cancer [1]. In addition to being the most common cause of cancer-related deaths worldwide for both men and women, this kind of cancer is most common in men [2–3].

The greatest incidence rate of lung cancer, 13%, was recorded in 2012 and rose to over 18% in 2015, making it the most common cancer globally [2]. In Australia, lung cancer was one of the top four cancer forms diagnosed in 2007. Approximately 3,755 women and 5,948 men received a lung cancer diagnosis in that year [4].

Approximately 80% of instances of lung cancer are caused by cigarettes, making smoking the primary risk factor for both active and passive smokers [2]. Air pollution, chemicals (paint materials, chemical waste, asbestos, radon), unhealthy foods (such as junk food and satay), jobs that expose people to carcinogens (painters, construction workers, drivers), alcohol consumption (>30g/day), a family history of cancer, a history of pulmonary disease (tuberculosis, asthma), and a lack of physical activity are additional risk factors for lung cancer [5,6].

There are two forms of lung cancer: non-small cell lung cancer (NSCLC) and small cell lung cancer (SCLC) [1,7,8]. SCLC and NSCLC are two distinct illnesses that should be viewed as such based on their clinical course [7]. According to studies, NSCLC accounts for more than 86% of lung cancer incidences [1, 8]. The growth rate of NSCLC is slower than that of SCLC. Slow growth rates are typically harmful because they often don't show

any signs until they are advanced. Large-cell undifferentiated carcinoma, lung adenocarcinoma, and squamous cell carcinoma are the three primary forms of non-small cell lung cancer [9].
Lung cancer treatment is typically complex and involves a variety of treatment modalities, such as surgery, radiotherapy, palliative care, systemic therapies (such as chemotherapy, immunotherapy, and targeted medicines), and interventional radiology [10]. Even with the quick advancement of treatment technology and the availability of more treatment options for this aggressive malignancy, survival rates are still low, especially for lung cancer that has spread locally and metastatically [3].
The only treatment modality with indications for all disease stages and patient performance status categories is radiotherapy [10]. Due to tumor motion caused by the heart and lungs, the lung's low electron density, and the proximity of vital organs including the esophagus and spinal cord, the thorax continues to be a difficult anatomical site for radiation therapy. Nevertheless, many of these issues can be resolved by sophisticated radiation technologies [11], which will enhance the course of treatment for lung cancer [10]. However, in many regions of the world, radiation is currently underutilized [10].
The clinical benefit of such technology still needs to be proven because radiation oncology is a medical specialty with extremely large Medicare expenditures [12]. Therefore, the purpose of this study was to examine how radiation therapy for lung cancer affects lung inhomogeneity density and dosage variations.

2. MATERIAL AND METHODS

The methodology used in this investigation was divided into two parts. A computerized care planning system was used for the first section's configurations and procedures. Using an ionization container as a baseline, phase two of the setup was used to gather experimental results following the correction of the system's primary data.

2.1 Procedure for the TPS which is (Computerized Treatment Planning System)

The Pinnacle 3 treatment planning framework from Philips Healthcare in the Netherlands is shown in Figure (1). Its purpose is to collect data for the computerized treatment planning framework. The University of Wollongong is the owner of the Pinnacle3 software utilized in this investigation.

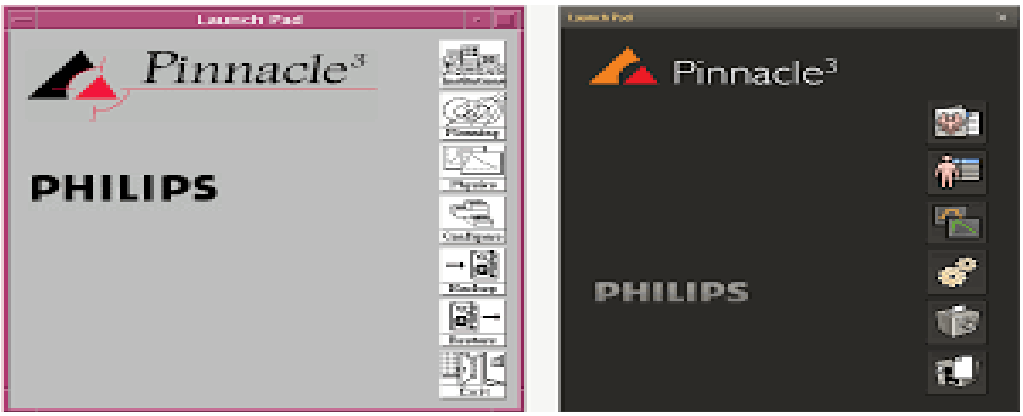

Figure 1: Pinnacle3 Employed in This Research

With the granularity of the dosing matrix established at 2 mm and the width and depth of the entire area set at 25 cm, the dosage grid was enlarged to cover the full region. For both narrower and broader gaps, it is known that the dose is appropriately calculated between matrix nodes because incorrect insinuate estimation would result in an incorrect dose, especially in penumbra sections, build u regions, and interfaces. Therefore, at the beginning of the grid size specification, a suitable number should be chosen, and the outcomes should be assessed to make sure the grid dimension is functioning properly.
Optimizing the interpolation method for calculating dosage between grid points and aligning the coordinate system where the dose computation locations are defined in both the image and machine coordinate systems are particularly crucial when using continuous and/or irregular grid spacing.
There are three parts to the phantom. Additionally, they can penetrate 25 cm in total. The density of the first portion (POI1) is 1 g/cm3, and its depth is 5 cm. Although the second region's density (the lung phantom) may vary, it typically falls between 5 and 15 cm deep. The third area's (POI3) depth might vary from 20 to 25 cm. Two radiation intensities, 6MV and 10MV, were employed in this study in the SSD (source to surface distance) at 100 cm in accordance with the ECWG measurement values. When determining the dosage dissemination and yield element for electron radiations, the SSD is essential.
The sizes of fields vary from 3 cm by 3 cm to 5 cm by 5 cm to 10 cm by 10 cm. The close relationship between radiation dosage and field size makes it possible to identify the pertinent patient sections.

The various numbers used to experiment with the phantom's density in order to examine the effects of density fluctuation were 0.1 gm/cm3, 0.2 gm/cm3, 0.3 gm/cm3, and 0.4 gm/cm3. The effects of photons' mass density are demonstrated by the mass attenuation and absorption coefficients. As a result, the density of the media that will be exposed to radiation and the dosage calculation have a strong link. Additionally, the four different densities were simulated using 10 MV, and the three different field widths were exposed to radiation of 6 MV energy simultaneously.This assignment's necessary setups ought to be saved for the procedures in part two. As part of this procedure, several data sets were gathered for different lung densities and field sizes. The tolerance between the simulation produced by Pinnacle3 and the actual experimentally established standard values was compared using the same data analysis.

2.2 Experimental Procedure

Every layout from the initial stage is still accessible. Figure (2) depicts the test arrangement at Wollongong Hospital using the Varian 21Ex Linear Accelerator (Linac). Additionally, in these studies, dose changes were detected using ionization chambers.

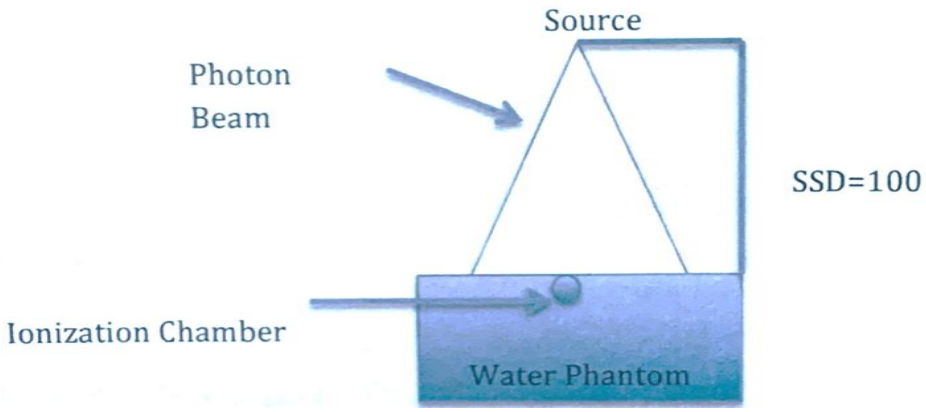

Figure 2: the experimental setup for initial measurement.

A number of preparatory steps must be taken to guarantee that the LINAC settings satisfy the treatment specifications. Making ensuring there is a 1mm run out in the collimator rotation is the first step. To make sure that the run-out is less than ±1 mm off the norm, it is also essential to evaluate the gantry rotation. Next, determine whether the table rotation deviates by ±1 mm from the baseline. Less than 1 millimeter of laser alignment tolerance is another requirement. The LINAC's maximal efficiency has thus been confirmed, and these assessments served as the benchmarks for the commissioning procedure.In the second stage, the solid water phantom needs to be in the isocenter. The isocenter and a standard SSD (of 100cm dimension) should be used to determine the midpoint of the measuring ionization chamber. Every size should also be standardized to a specific depth.

Additionally, it is recommended that the reference ionization chamber be positioned beneath the field size and at different desired places. One of the pieces that comprise the solid water phantom has a complete figure (3). You can choose from a range of depths by dragging this piece along the phantom. Consequently, this aperture allowed the ionization chamber to enter the solid water phantom. The commissioning procedures serve as the basis for these inspections, which confirm that the measuring apparatus is accurate and capable of serving as standardized settings for obtaining trustworthy results.

Figure 3: shows the initial evaluation setup utilizing an ionization chamber

Figure 4 depicts a CC04 conventional ionization chamber. Studies examining the ling reciprocal dose in radiation made use of this ionization chamber. This ionization chamber was also utilized to quantify the central axis absorbed dosage in a heterogeneous lung phantom. Using a measure of water density P=1g/cm3 and a minimal lung density P=0.3g/cm3, a robust apparition of "water" was employed. A variety of distances were investigated, and 6MV and 10MV of energy were employed to determine the depth. This study uses three different field dimensions: 3 cm x 3 cm, 5 cm x 5 cm, and 10 cm x 10 cm. We examined how accurate, from the perspective of the treatment planning paradigm, the dosage quantity was using the ionization chamber approach as a reference (Pinnacle3).

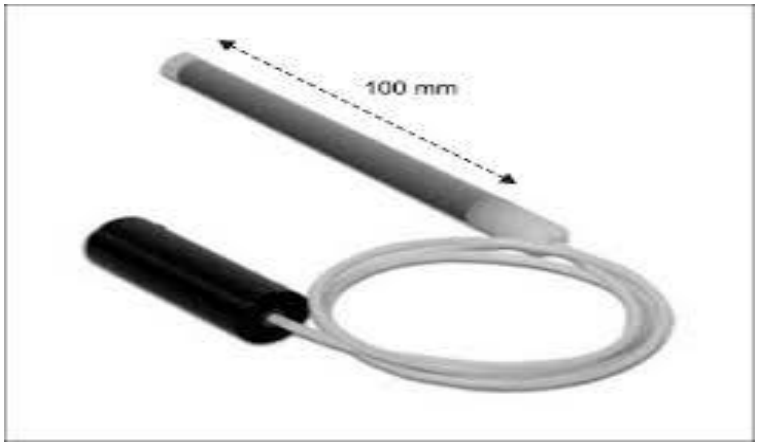

Figure 4: the Ionisation chamber (CC04)

2.3 Methods of Dose Calculation

In this study, the Pinnacle3 3D treatment planning framework was used. Additionally, the lung apparition dose distribution was estimated using a (CCCS) technique.

The CCCS dose model, which takes into account primary photon incidence, secondary electrons, and heterogeneity issues in lung areas, aids in obtaining an accurate three-dimensional dose estimate. The CCCS technique can be used to evaluate the dose distribution in components that may be experiencing an electrical imbalance, such as the lungs' air cavity. The main goals of the treatment planning system—reliable determination and low time cost—are met by the CCCS dose model.

2.3.1 Convolution Superposition Dose Model

Pinnacle3's CCCS dosing algorithm architecture was based on the Mackie et al. technique. The CCCS algorithm determines dose distributions using first-principles calculations rather than corrective factors to enhance dose allocation estimations. It can now take into account how radiation modulator, external patient shapes, and inhomogeneous tissue affect dose distribution [13].

The CCCS dosing algorithm cannot begin without the following procedure. The accelerator's head serves as the source of the incident photons, which must first be modularized. The second step involves determining the TERMA (Total energy Released per unit Mass) volume as this energy penetrates the patient's sample density in the projection. Lateral scatter, including the impact of heterogeneities across the TERMA's energy implantation kernel in three dimensions, is monitored using the ray-tracking technique. In the end, we contaminate the projected photon dosage distribution even though the electrons have been medialized and decline sharply.

2.3.2 Adaptive Convolution Superposition

With a few adjustments to the computation techniques, Pinnacle3 also uses the adaptive convolution superposition (ACS) technique. A coarse 3D grid with dosage distribution was used in conjunction with the TERMA for evaluation. At the intermediate stage, the computer provides a high-resolution dose allocation with respect to the upper part of curvature. The computer then dynamically enhances the resolution change in the region with a higher curvature.Having said that, the resolution needs to be excellent enough to be taken into account for this. In the case of the lower curvature area, the dose distribution enters from the coarse dosage grid. Additionally, the adaptive convolution superposition (ACS) method reduces computing time while maintaining the accuracy of the CCCS calculation despite tissue heterogeneities.

3. RESULTS

Using CCCS calculations, results from the Treatment Planning System Pinnacle3 were examined to examine the impact of density fluctuation for different field dimensions and irradiation intensities.

3.1 Depth-dose characteristics for a diverse apparition at 6 and 10 MV and different area dimensions in varied lung apparition concretions

The following data display the percentage of comparable dosage vs depth in centimeters. From the surface of the phantom down to a depth of 5 cm, the density of the human body was estimated using water with a concretion of 1 g/cm3. The figure shows lungs of different densities with densities ranging from 0.1, 0.2, 0.3, and 0.4 g/cm3, with curves spanning from 5 cm to 15 cm (for depth). The human body's perimeter, which is composed primarily of water with a concretion of 1 g/cm3, is represented by the extra depth between 15 and 25 cm.

For the evaluation, a radiation intensity of 6MV and field dimensions of 3 cm x 3 cm were used to get the answer in the curve. Figure 5 illustrates how the relative percentage of absorbed dosage decreases with increasing depth. The lung, a medium with a lesser density, showed a higher percentage of reduction than the water media. The graph showed that the proportional dose decreased with decreasing density, with 0.1 g/cm3 having the lowest proportional dose. The 0.2 g/cm3 was followed by 0.3 and 0.4 g/cm3, although in contrast to the two-water media, the 0.3 and 0.4 g/cm3 displayed a minor shift in the absorption slope.

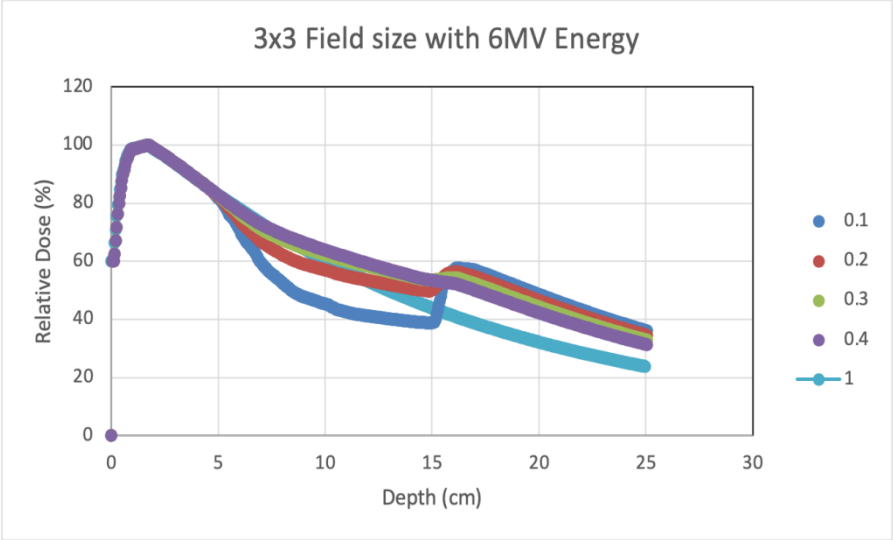

Figure 5: A composite apparition's depth-dose characteristics at 6MV and a field dimension of 3cmx3cm in varied lung apparition densities (0.1, 0.2, 0.3, and 0.4) g/cm3.

The depth-dose characteristics for a varied apparition at 6MV with a 5 cm × 5 cm area dimension at different lung apparition concretions are then displayed in figure (6). The 6MV with 5 x 5 cm area dimension and the 3 x 3 field dimension with 6MV radiation intensity delivery have the same tendency in aqueous media with 1 g/cm3. One variable is the alteration in the lung medium, which in this case was more noticeable at 0.1 g/cm3.

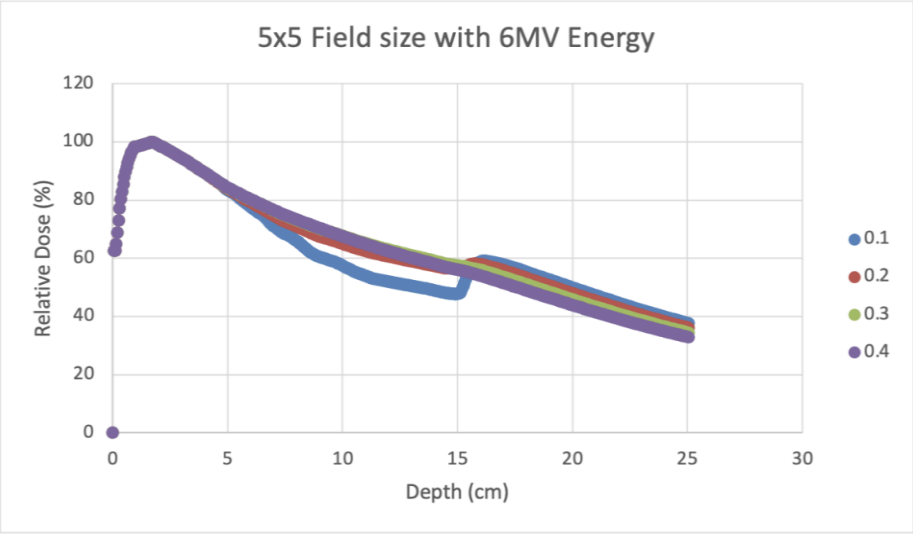

Figure 6: Depth-dose characteristics for a diverse apparition at 6MV with a 5cmx5cm area dimension at various lung apparition concretions (0.1, 0.2, 0.3, and 0.4) g/cm3.

Figure 7 displays the depth-dose characteristics for a variety of lung apparition concretions (0.1, 0.2, 0.3, and 0.4) g/cm3 in a heterogeneous apparition at 6MV with an area dimension of 10 cm × 10 cm. With a field dimension of 10 cm × 10 cm and the same radiation intensity delivery of 6MV, it is evident that there is no discernible change in density in the lung media.

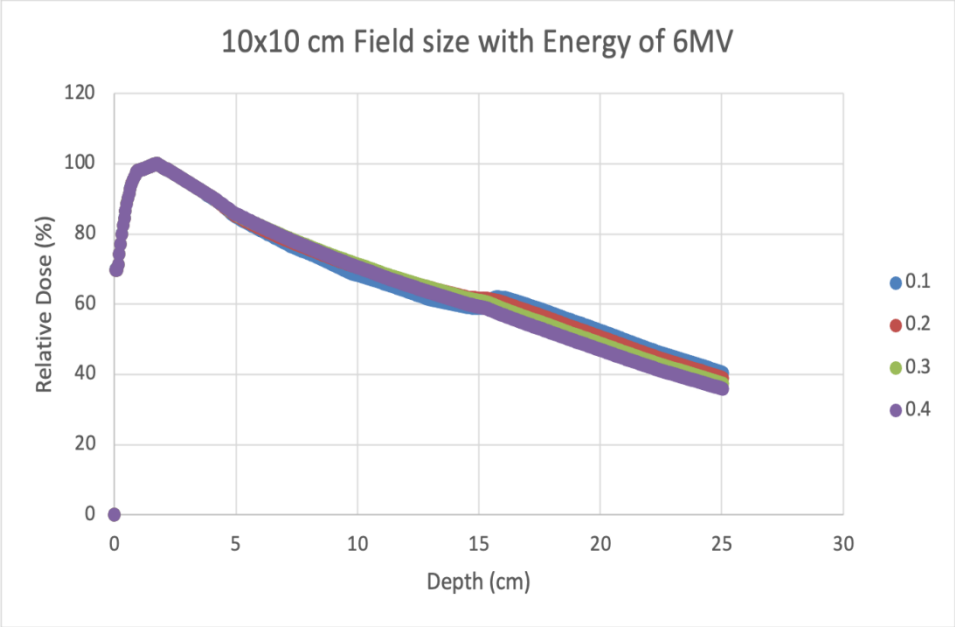

Figure 7: Depth-dose characteristics for a diverse apparition at 6MV and an area dimension of 10cmx10cm in varied lung apparition concretions.

The next figure displays the depth-dose characteristics for a variety of lung apparition concretions (0.1, 0.2, 0.3, and 0.4) g/cm3 with an area dimension of 3 cm x 3 cm and a heterogeneous apparition at 10MV. Absorption was significantly reduced in the lung media for the 0.1 g/cm3 density. The lung and lower body (water) mediums did not have the 0.3 g/cm3 or 0.4 g/cm3 values.

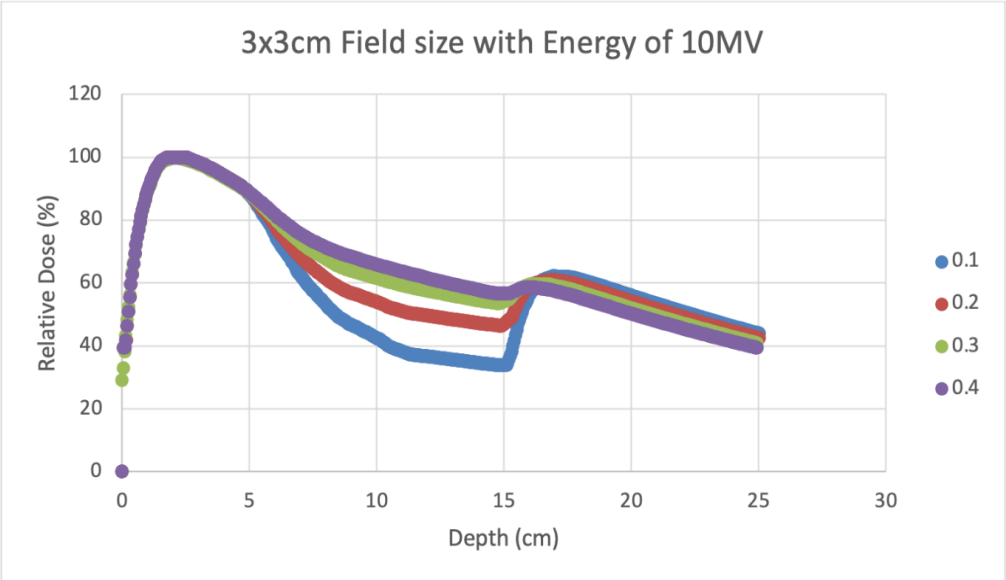

Figure 8: Depth-dose characteristics for a diverse apparition at 10MV and an area dimension of 3cmx3cm in varied lung apparition concretions.

The depth-dose parameters for a heterogeneous apparition at 10MV with a 5 cm × 5 cm area dimension in various lung apparition concretions (0.1, 0.2, 0.3, and 0.4) g/cm3 are displayed in Figure 9. It is evident that the lung media had a lower percentage of absorption at concretions of 0.1 and 0.2 g/cm3. There was no discernible variation in the absorption ratio between densities of 0.3 and 0.4 g/cm3.

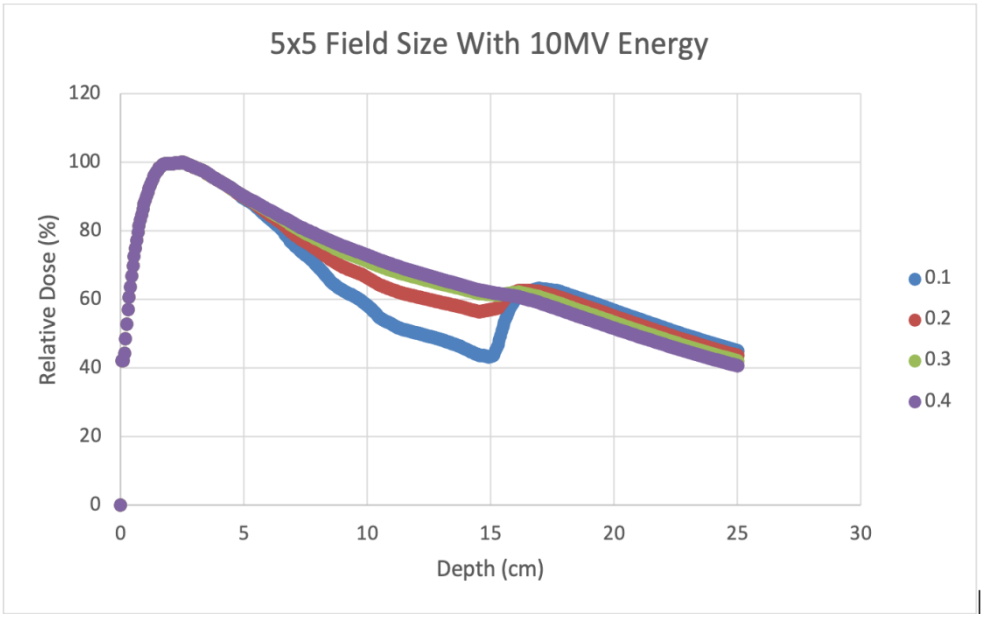

Figure 9 : Depth-dose characteristics for a diverse apparition at 10MV and an area dimension of 5cmx5cm in varied lung apparition concretions.

Figure 10 illustrates that a field dimension of 10 cm x 10 cm received a radiation energy of 10 MV. There is a general pattern in the absorption ratio for the densities, with the exception of the 0.1 g/cm3 in the lung medium, where the percentage of absorption was decreased.

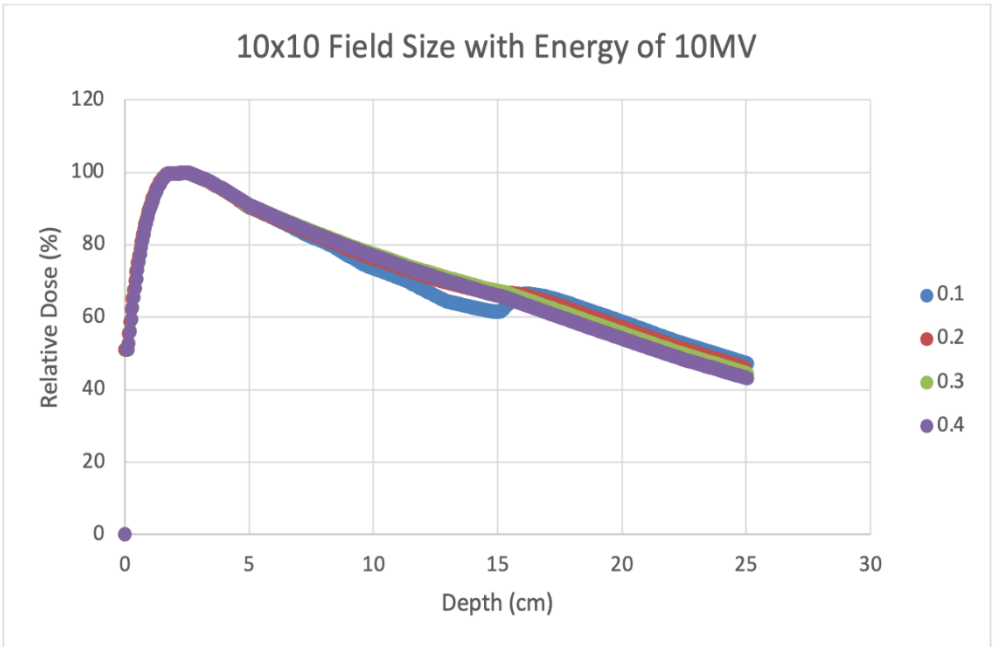

Figure 10: Depth-dose characteristics for a diverse apparition at 10MV and an area dimension of 10cmx10cm in varied lung apparition concretions.

3.2 As benchmark, the different results of ICM which is Ionisation Chamber Measurement and TPS CCCS. Using TPS CCCS and Ionization Box Assessment as a baseline and contrast the findings.

The arithmetic means of the concretions used in Pinnacle3 were chosen for this correlation phase and found to be 0.3 g/cm3. A 5% accuracy margin was taken into consideration for this investigation.

A heterogeneous phantom with an average density of 0.3 g/cm3 inside the lung media and a beam intensity of 6MV blasted through a 3 cm × 3 cm field dimension was used to compare the results in figure 11. The graph showed that pinnacle3 and the ionization container were in accord at all depths.

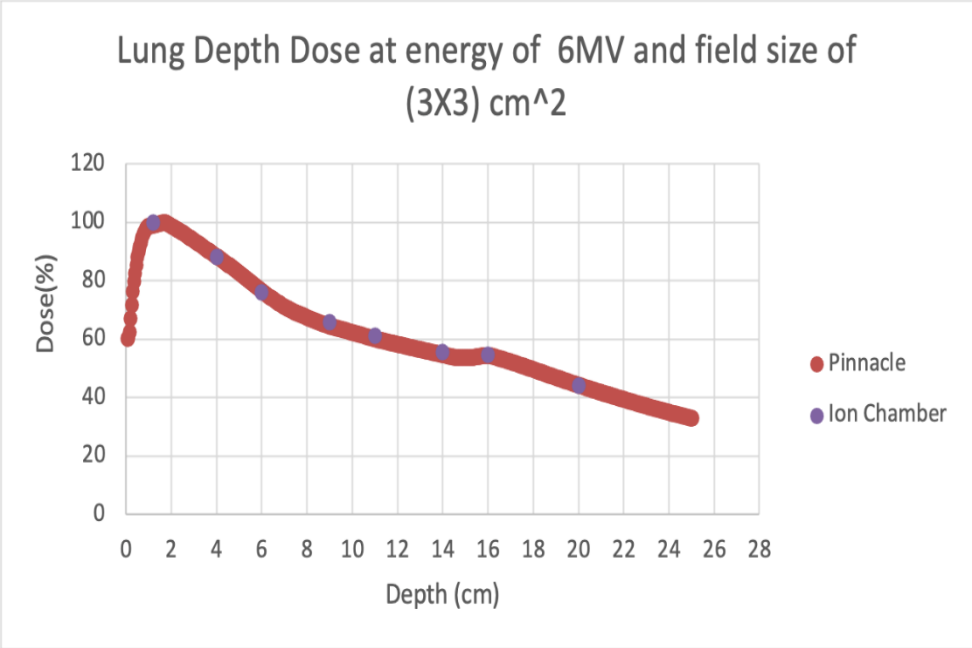

Figure 11: comparison findings from the benchmark ionization chamber and the treatment planning simulation Pinnacle3 CCCS, at the identical radiation energy of 6MV and the same field dimension of 3cmx3cm

The results from the treatment planning simulation Pinnacle3 CCCS and the benchmark ionization chamber are compared in the following figure with the same radiation energy of 6MV and field size of 5 cm x 5 cm. Figure 12 displays the calculated and observed results; however, in this case, a 6MV energy radiation was emitted using a field dimension of 5 cm x 5 cm. The average density for the heterogeneous phantom was 0.3 g/cm3. The graph showed consistency between the ionization chamber and pinnacle3 at all depths.

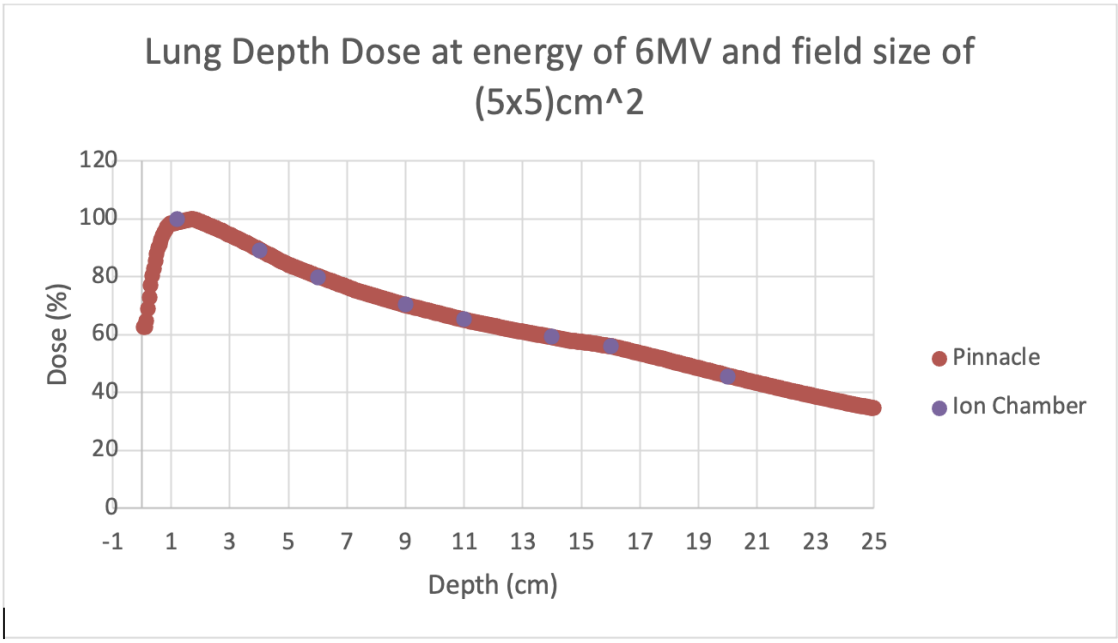

Figure 12: comparison the findings from the benchmark ionization chamber and the treatment planning simulation Pinnacle3 CCCS, at the identical radiation energy of 6MV and the same field dimension of 5cmx5cm.

Figure 13 compares the estimated and observed results for the same condition of 0.3 g/cm3 density for various apparitions, radiation intensity of 6MV, and area dimension of 10 cm × 10 cm. The study's findings showed that, at every depth of observation, the predicted dose using the CCCS computing technique was well within the standard error of the ionization chamber.

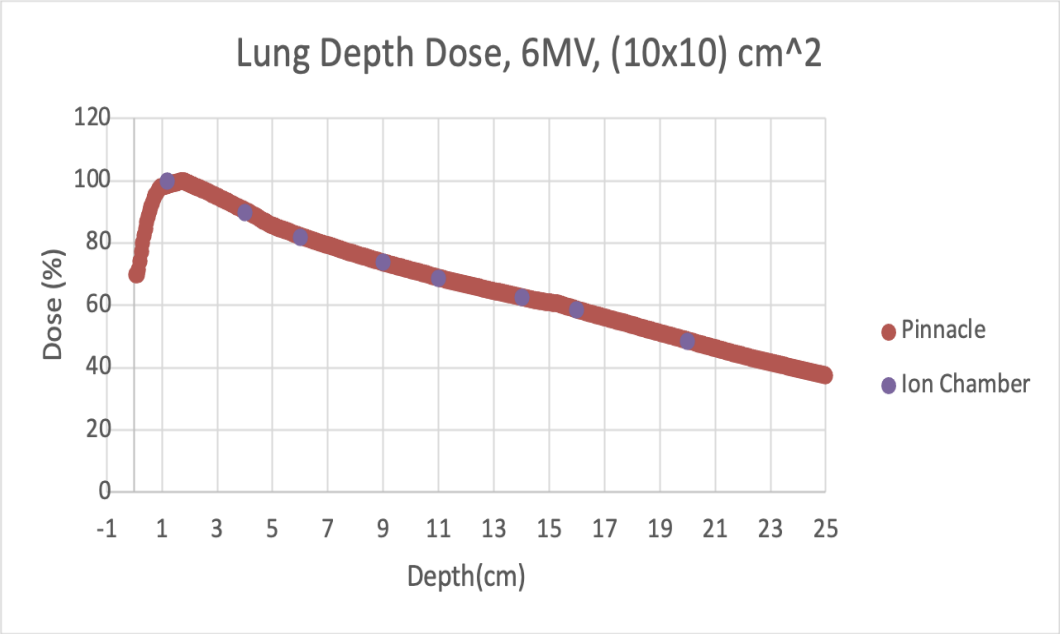

Figure 13: at the identical radiation energy of 6MV and the same field dimension of 10cmx10cm, the findings from the benchmark ionization chamber and the treatment planning simulation Pinnacle3 CCCS were compared.

Figure 14 compares the computed and observed results under the same conditions of 0.3 g/cm3 density for heterogeneous phantom, beam intensity of 10MV, and field size of 3 cm × 3 cm. The graph shows a subtle difference between the ionization box and pinnacle3 results for the phantom at a heterogeneous low-density material. Consequently, there is a slight difference between the ionization chamber and pinnacle3 results.

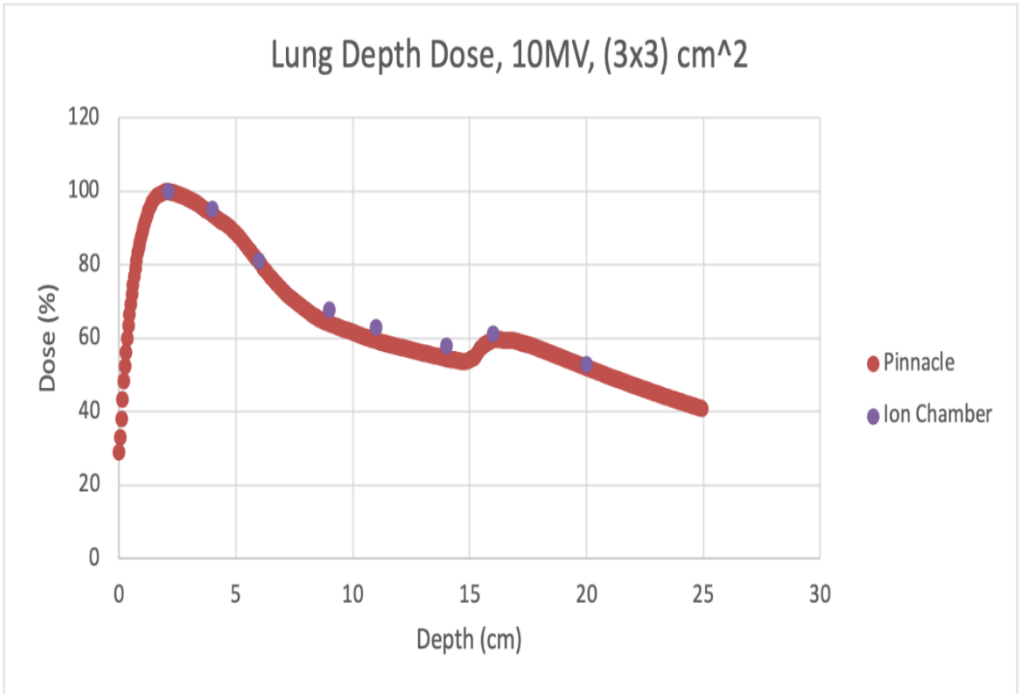

Figure 14: at the identical radiation energy of 10MV and the same field dimension of 3cmx3cm, the findings from the reference ionization chamber and the treatment planning simulation Pinnacle3 CCCS were compared.

With the exception of depths of 14 and 16 cm, where there is some inaccuracy since the observed result was somewhat higher than the CCCS simulation results, the low-density material, as shown in figure 15, accords with the CCCS assessment at all levels. This test was conducted with a 10 MV beam intensity, a 5 cm × 5 cm field, and 0.3 g/cm3 of heterogeneous material, despite.

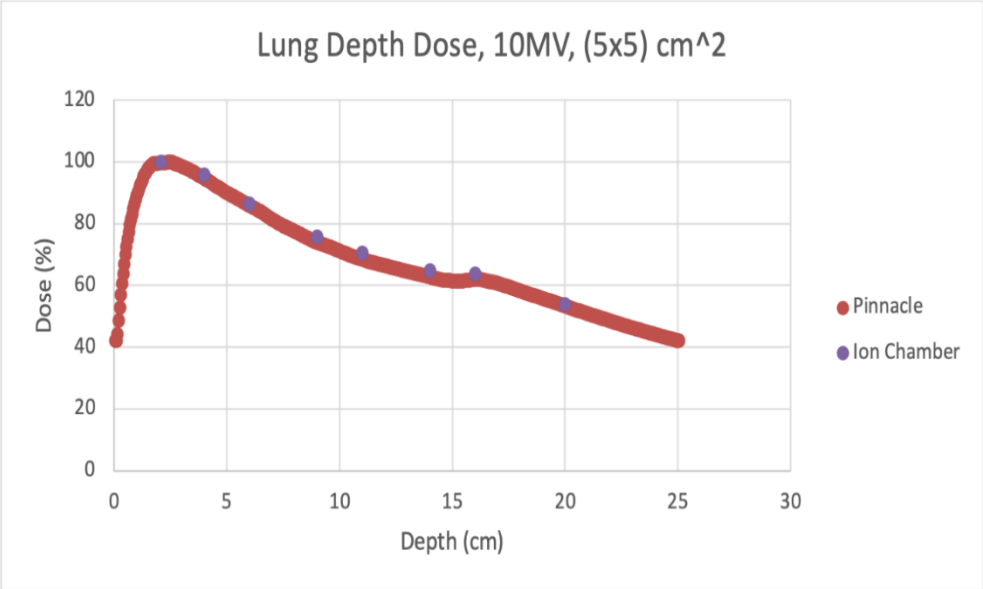

Figure 15: comparison of the results gained from the standard benchmark ionisation chamber and the treatment planning simulation Pinnacle[3] CCCS for the beam energy 10MV with the field size being at 5cm x 5cm are made.

The results of the ionization container and the CCCS simulation utilizing 10MV of beam intensity given through a field dimension of 10 cm × 10 cm are compared in Figure 16. Pinnacle 3 and the ionization compartment were in harmony at all depths.

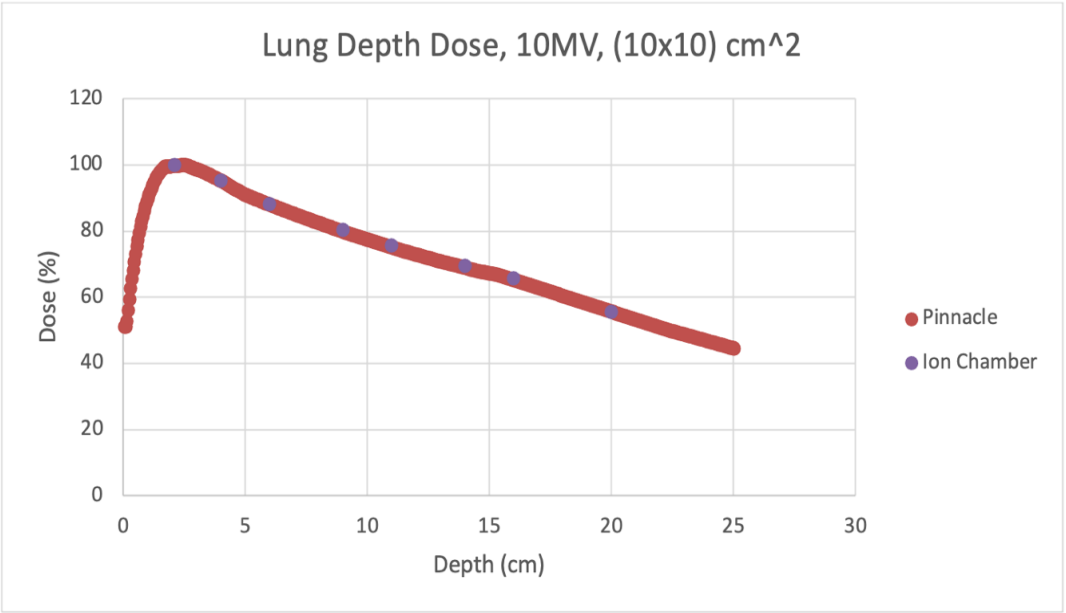

Figures 16: comparison the results gotten from the benchmark ionisation chamber and treatment planning simulation Pinnacle[3] CCCS for the beam energy of 10MV and a field size 10cmx10cm.

3.3 Curves of Isodose Comparison

Figure 17 compares the isodose curves at three different field sizes (3x3 cm, 5x5 cm, and 10x10 cm) with the same beam energy (6MV) and heterogeneous density (0.3 g/cm3). For every field size, a symmetrical dosage profile was observed. Over the penumbra region, the curve stayed smooth. The profile lost its flatness at the 3x3 cm and 5x5 cm field size edges. The penumbra's overall variance was only 5%, which is negligible. Lastly, there was a slight variation of around 20% between the ORA% of 3x3 cm and 5x5 cm.

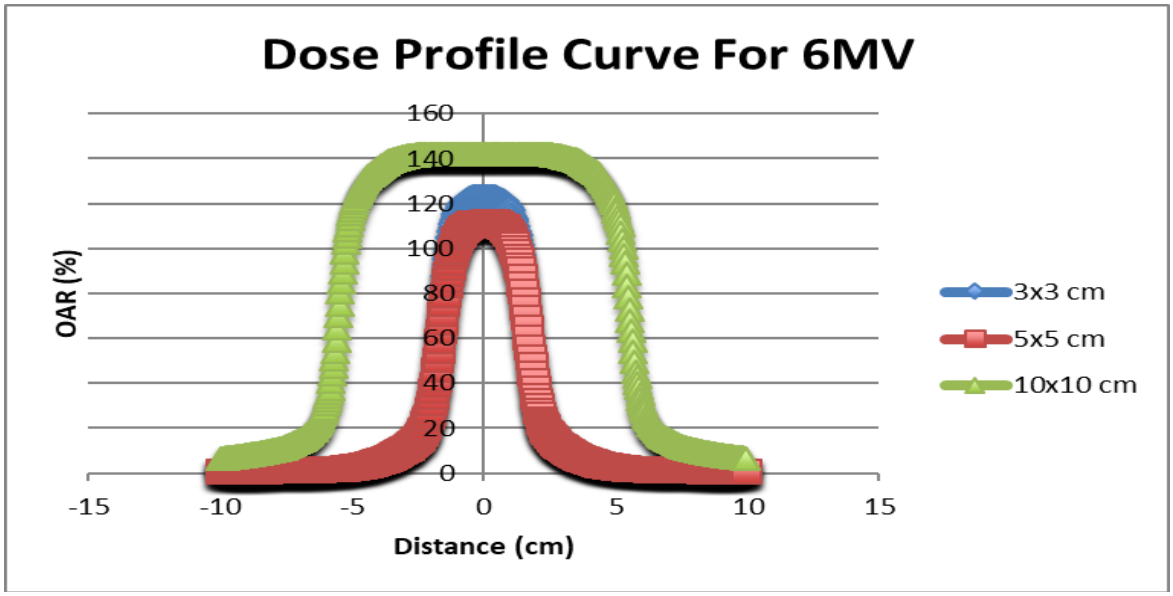

Figures 17: Isodose curves gained at the beam energy of 6MV for 3 cm x 3 cm, 5 cm x 5 cm and 10 cm x 10 cm at a density of 0.3 g/cm^3 are given in the figure 4-13

Figure 18 shows the evolution of the dose profile curve using the same beam energy of 10 MV for field sizes of 3x3 cm, 5x5 cm, and 10x10 cm. A constant heterogeneous density of 0.3 g/cm3 was employed. The penumbra region was determined to be smooth overall, but only the 10x10 cm field size was discovered to lose the profile's flatness. For each of the three field sizes that were described, the dose profile was symmetrical around the Y-axis. The difference in ORA% between 3x3 cm and 5x5 cm was larger, at almost 40%, whereas the variance profile in penumbra was smaller, at about 10%.

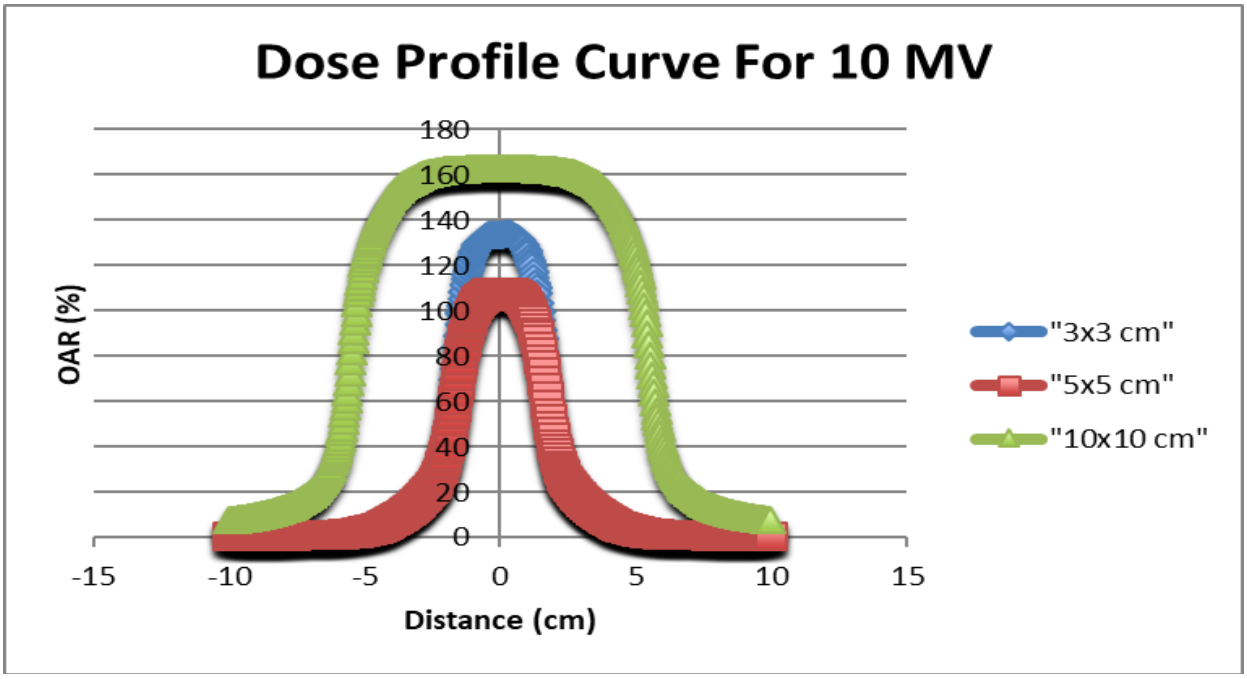

Figure 18: Isodose curves for the beam energy of 10MV for the field size 3 cm x 3 cm, field size 5 cm x 5 cm and field size 10 cm x 10 cm at a density of 0.3 g/cm^3.

3.4 The Influence of Field Size

Figure 19 illustrates this. Field sizes of 3x3 cm, 5x5 cm, and ultimately the 10x10 cm a6MV energy beam were employed for irradiation. The depth of the lung medium, which had a heterogeneous density of 0.3 g/cm3, ranged from 5 to 15 cm. The 10x10 cm and 5x5 cm field sizes showed negligible variations in absorbed dosages. Lastly, the absorbed dose for the 3x3 cm field size changed little.

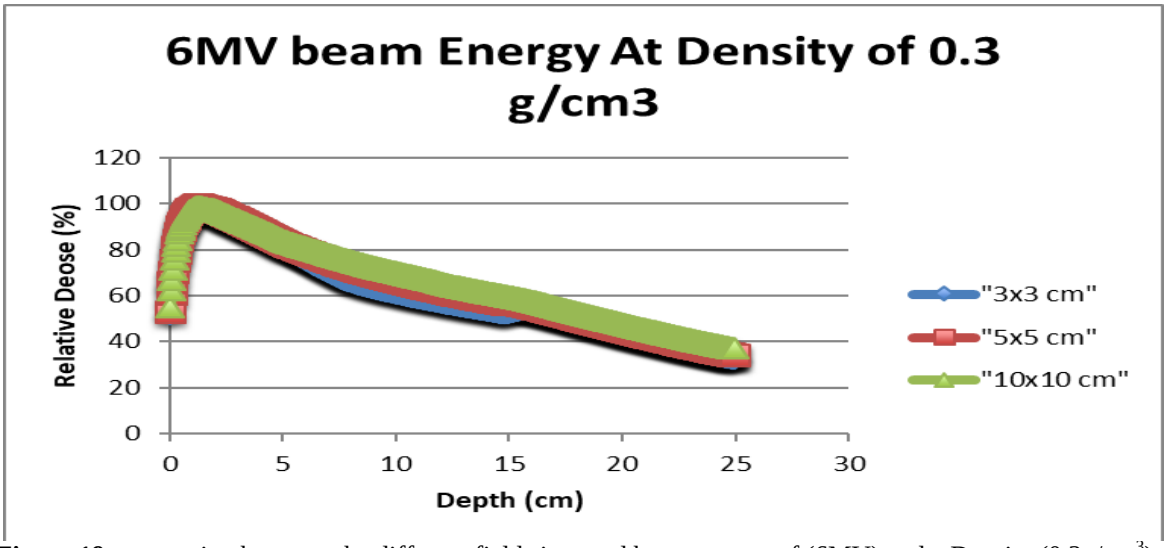

Figure 19: comparing between the different field sizes and beam energy of (6MV) and a Density (0.3g/cm^3).

Figure 20 also displays the relative dose absorbed as a proportion of depth. With a heterogeneous density of 0.3 g/cm3, the lung medium is represented at a depth of 5 to 15 cm. The three distinct field sizes—3x3 cm, 5x5 cm, and 10x10 cm—were exposed to 10MV radiation and put to use. Each of the various field sizes has a different curve according to the algorithm. When viewed via the lung phantom, the 10x10 cm field size exhibited no discernible influence, the 5x5 cm field size showed a very minor impact, and the 3x3 cm field size indicated a considerable impact of absorption.

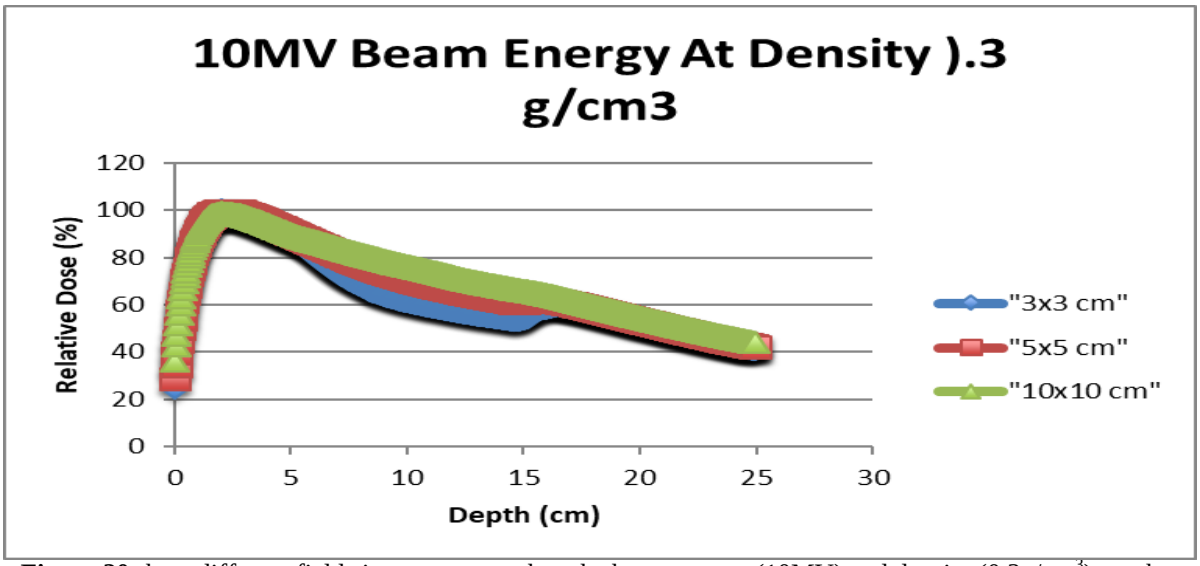

Figure 20: how different field sizes compare when the beam energy (10MV) and density (0.3g/cm^3) are the same.

3.5 The Power of Energy

4.5.1 Comparison Between energies being used in the TPS using CCCS

CCCS was utilized to compare the relative absorption for 6MV and 10MV pinnacle3 against depth. The result of the comparison using constants, which are a 3x3 cm field size and a heterogeneous density of 0.3 g/cm3, is shown in Figure 21. As illustrated in figure 4-17, the decline in 6MV pinnacle3 dosage absorption begins before it reaches the lung medium, which is located between 5 and 15 cm below the surface. The dose absorption for the 6MV beam energy increased, if little, near the end of the lung media, which is about 15 cm deep. The reduction begins at a depth of around 2 cm and continues. The decline in dose absorption for the 10 MV beam energy scenario began at a depth of approximately 4 cm, reached its maximum at 15 cm, then rose slightly to 16 cm before continuing to fall for the rest of the graph.

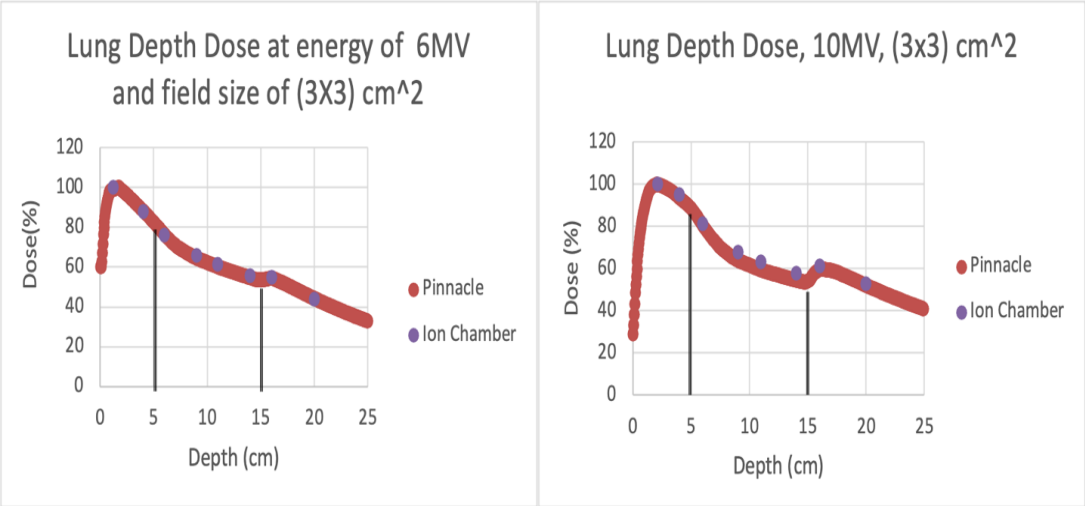

Figure 21: a comparison between two energies 6MV and the 10MV for the same field size of 3cm x 3cm and density of 0.3g/cm^3.

With the variable being the heterogeneous density of 0.1 g/cm3, the same beam energies of 6MV and 10MV, respectively, were compared for the same field size of 3x3 cm in figure 22. Both the 6MV and 10MV dose absorption began to decrease at a depth of roughly 2 cm, with the lowest point happening at the lung medium between 5 and 15 cm. The beam energy instantly entered the water medium after reaching a depth of 15 cm. The dosage absorption for both beam energies then began to rise until it reached a depth of 16 cm, at which point it began to decrease.

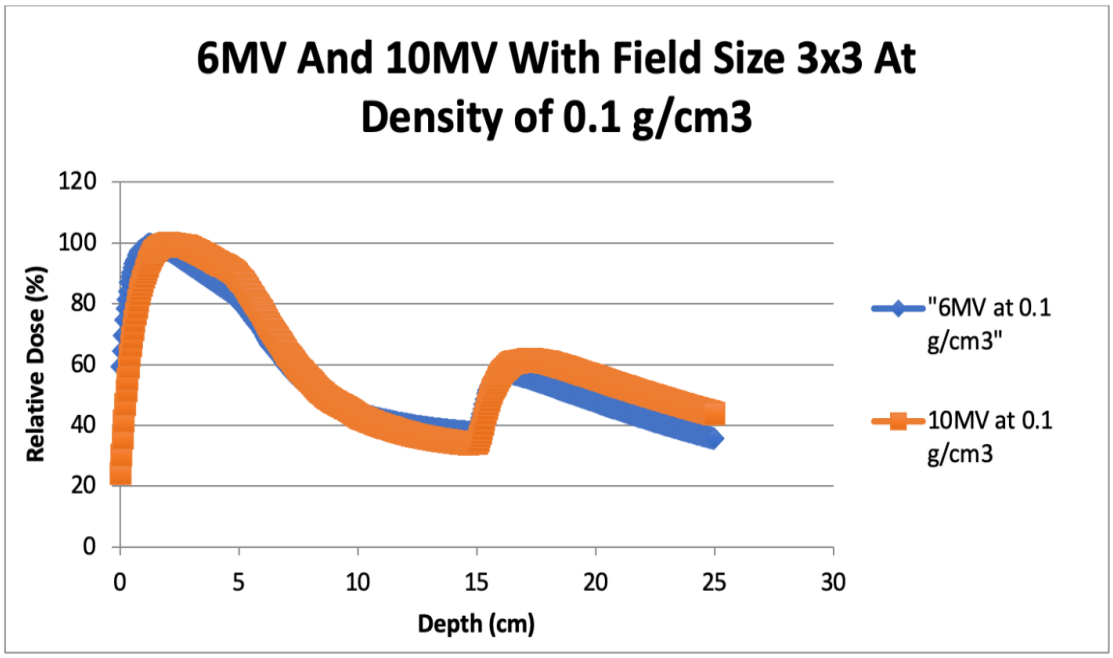

Figures 22: a comparison among the two energies 6MV and 10MV for the same field size 3cm x 3cm and density of 0.1g/cm^{3}is made.

3.5.2 The results of the CCCS and the Ionization Chamber are compared in terms of energy

In figure 21, a 6MV pinnacle3 was contrasted with a 10MV pinnacle3, and a CCCS at a 6MV ionization chamber was contrasted with a CCCS at a 10MV ionization chamber. The 3x3 cm field size and the 0.3 g/cm3 heterogeneous density served as the comparison's constants. The dosage found at 6MV ionization chambers and the dose absorbed at 6MV pinnacle3 were identical. The absorbed radiation at 10MV of the ionization chamber did not match the dose absorbed at 10MV pinnacle3. Furthermore, there was initially a little discrepancy between the 10MV ionization chamber and the 10MV pinnacle3, which diminished as the beam energy passed through the lung media.

Table 1: The percentage of dose absorbed at the nearest depth point towards the middle (10.99cm) in the phantom of the lung via the simulation by Pinnacle3 and the percentage of dose absorbed at nearest depth point towards the middle (11cm) of the lung phantom through the measurements on the ionization chamber.

	Pinnacle3			Experimental		
	3x3 cm	5x5 cm	10x10 cm	3x3 cm	5x5 cm	10x10 cm
6MV	60.1	65.1	68.9	61.2	65.4	68.7
10MV	59.4	68.5	75.1	63.0	70.7	75.6

According to table 1, a depth of 10.99 cm CCCS was chosen for the algorithm, and a midway point of 11 cm CCCS was applied. This spot was chosen because it was within the heterogeneous density of 0.3g/cm3 and in the middle of the lung phantom.

The following formula tabulates the values in table 2 and illustrates the difference in dosage measurements between the ionization chamber and the CCCS.

$$\%\text{Dose Different} = \frac{D_{ion-ch} - D_{conv}}{D_{ion-ch}} \times 100$$

Table 2: The relationship between calculation in the TPS pinnacle3 and the measurements done in ionization chamber from table 1

	% Dose difference		
	3x3	5x5	10x10
6MV	1.681675	0.334618	-0.28896
10MV	5.828941	3.026936	0.54621

Table 2 displayed the percentage dose variation for beam strengths of 6MV and 10MV. The largest % dose variance was 5.828941 percent while using 10MV beam intensity with a field dimension of 3x3 cm, whereas the percentage dose variation for 5x5 cm and 10x10 field dimensions was 3.026936 percent and 0.54621 percent, respectively. The field size grows when 6MV beam intensity is used, while the dosage variation percentage falls. When the field size was 10x10 cm, the dosage differential was -0.28896 percent; when the field size was 5x5 cm, it was 0.334618 percent; and when the field size was 3x3 cm, it was 1.681675 percent.

4. DISCUSSION

In this work, the convolution calculation approach was used to determine the necessary changes in radiotherapy radiation doses due to changes in lung homogeneity and density. The treatment planning system (TPS) and this calculating approach were compared. A comparison between the estimated and measured isodose lines for a heterogeneous medium comprising lung media and water was used to assess the calculation accuracy for the dose CCCS [14]. The average disparity between the calculated and measured doses for the symmetric fields was only 3.5%.

The following metrics were used in this work: a heterogeneous phantom density of 0.1 g/cm3 for the lung media, 0.2 g/cm3 for the first water medium, 0.3 g/cm3, and 0.4 g/cm3 for the second water medium; a radiated beam intensity of 6MV and 10MV. The results of the ionization compartments for the two-beam intensities across the medium were also compared in this investigation. The findings and relative evaluation of the differences are reliable because the errors in this research work are within the recommended limits, whereas the International Commission on Radiation Units (ICRU) accepts a maximum of 5% computation errors at a low density of 0.3 g/cm3, narrow field dimensions, and high beam power. Beam intensity, density medium, and field dimensions all have an impact on dosage allocation and assimilation; therefore, the analysis of the results focused on the accuracy of the CCCS using the variables used as a baseline [15].

4.1By using Collapsed Cone Convolution Superposition (CCCS) to calculate the doses.

Such a tendency as observed in the graphs for low-density medium, which is the lung medium, may have resulted from disturbances that are by nature energy and density-dependent, which may have affected the fluctuations and accuracy that are evident in the dosage calculation. Pinnacle3 was utilized for tiny photon beams in order to collect the dosimetry data. In order to compare the accuracy of CCCS dose calculation methods, an

ionization chamber was used in this experiment [16]. When the beam energy reached the lung medium, the CCCS results were consistent with the 10MV beam energy through 5x5 cm and the 10x10 cm field size. This was the case for the first water medium, which was located at a depth of 5 cm. The CCCS method, which relied on pinnacle3, provided a uniform trend for the energy beams and the heterogeneous densities. These were, respectively, 3.026936% and 0.54621%, which are below the 5% maximum permitted difference. As indicated in Table 2, the exceptions were primarily observed in the 10MV 3x3 cm lung medium field sizes, with a dosage variation of 5.828941%. Concurrently, each of these differences took place at the center of each medium. The discrepancies in the attenuation coefficient, the beam energy absorption coefficient, and the collision stopping powers cause an interface error at the interface between one medium and another, such as at points 5 cm depth and 16 cm depth in figures 14 and 15.

Forward electronic disequilibrium (FED), which arises when the electron production on either side of the media differs from one another, is another possible reason for the inaccuracy. Prolapsing causes errors as a result of these variances. When using the 6MV beam of energy, the error that resulted from the underprediction of the dose distribution was below the acceptable range. It was - 0.28896% for the 10x10 cm field size, 0.334618% for the 5x5 cm field size, and 1.681675% for the 3x3 cm field size. All of these errors are displayed in Table 2.

Pinnacle3 values for the field of 10x10 cm size are significantly lower than the experiment's results for both the 6MV and 10MV beam energies when the absorbed dosage % is taken into account and potential errors are ignored. The experimental value is low for the field size of 10x10 cm in 10MV, which is a sign that, generally speaking, under all conditions, the experiment's results are especially linked to greater errors, ranging from human error to equipment variances and scaling.

With the exception of the 5x5 cm for 10MV, where it is not considered an error because it produces a negative percentage of -0.28896%, as shown in table 2, the experiment results obtained through the ionization chambers were higher than the results obtained from the method of the CCCS pinnacle3. According to these findings, the TPS's results, which employ the CCCS dose calculation algorithm, are considered to be accurate for all beam energy, medium densities, and field sizes [17].For the 10MV and 3x3 cm field size, the largest discrepancy between the Monte Carlo and Pinnacle3 findings is 5.828941%. This relatively large absolute dosage variance is oriented towards a significantly bigger difference in the percentage because of the large unconditional value of the dose. In contrast to experimental Monte Carlo methods that involve the use of ion chambers, this analysis shows that the Collapsed Cone Convolution Superposition method (CCCS) is accurate and a more consistent approach for calculating the dose absorption through the various media with heterogeneous densities.As an illustration, figure 21 shows a variation in the 10MV ionization chamber findings, which were completely out of sync with the 10MV and 6MV pinnacle3 at the low-density medium, which is thought to be the lung medium.

4.2 Effects of Density on Dose Distribution

The density of the media is the important factor that determines the rate of dose absorption when the different beam energy are irradiated. The figures 5, 6, 7, 8, 9, and 10 illustrate how density affects absorption dosage absorption. As can be shown from the figures and from all of the irradiation beam energy, the rate of absorption decreases at a low medium density between 5 and 15 cm, and this decline starts at the adjacent media border.A lateral electronic disequilibrium (LED) is created by the different electron numbers in the adjacent media when the beam energy passes through the interface and enters a medium with a low density. In contrast to the exit of the medium, where a large variety of secondary electrons are located, the absorption decreases quickly near the medium initiation. Because of the self-ionization that results from the electron's contact with the molecules, there are typically more electrons at the end of the medium than at the beginning. This indicates that the secondary electrons are crucial in relation to the density of the medium. As an illustration, a lower density medium has a wider range of secondary electrons that eventually reach a lateral electronic disequilibrium (LED), which lowers the doses recommended for lung tumors in the results of worldwide study.

Figures 17 and 18 display the isodose profiles of the beam energies for the 10 MV and 6 MV. One of the most important factors influencing the dosage profile is thought to be the medium's density. For instance, if the penumbra's breadth increases, it indicates that the beam energy is in a low-density medium.The density of the medium increases when the penumbra width decreases, indicating that the density of the medium is inversely related to the penumbra width. At low density, the rate at which the beam energy is absorbed by the tissues decreases as the depth increases due to the nearby motion of the charged particles.

4.3 Effect of Beam Energy on Dose Distribution

As shown in figures 21 and 22, the best analysis of the beam energies may be performed by comparing 6MV and 10MV with the different heterogeneous densities of 0.3 g/cm3 and 0.1 g/cm3. The study will have greater practicality after the medium density is incorporated. The relative dose absorption at an average density of 0.1 g/cm3 is lower than at 6MV in the lung medium but higher than at 6MV in aqueous media when exposed to a beam energy of 10MV. For instance, in a low density medium, the beam energy for the 10MV was 31.7%, while for the 6MV, it was 36.5%. One explanation is that the quantity of secondary electrons The rationale is that when

the beam intensity increases, the quantity of secondary electrons increases as well, leading to the creation of the LED that is responsible for lowering lung tumor dosages. High beam energy is seen as advantageous in high-density media because of its enormous impact, which enhances photon penetration and, consequently, the dosage absorbed, in comparison to a low beam energy of 6MV.In the case of the low medium, the 6MV is advantageous because it produces fewer LEDs, secondary electors, and a medium conclusion that increases the rate of dosage absorption in the tissues.

Figure 21 illustrates that a faster rate of ionization occurs in the low-density medium due to a higher beam energy of 10MV. At the lung medium, the ionization is likewise modest for a 6MV beam energy. Table 2 shows the dose absorption when a 6MV beam energy is irradiated under the appropriate maximum of 5%; however, in this instance, the error is regarded as being somewhat over the established bounds for the 10MV at 3x3 cm cm field sizes, with 5.828941% errors correspondingly. This indicates that when the given beam energy increases, the inaccuracy in dose absorption increases as well. According to the comparison of isodose curves shown in figures 17 and 18, the girth of the penumbra increases as beam energy increases.

4.4 Field Sizes Have an Impact

The field sizes used for the research in figures 19 and 20 are 3x3 cm, 5x5 cm, and 10x10 cm. This indicates that, when all other aspects in the study are taken into account, a larger field size leads to a higher absorption of the dose. Again, when a 6MV was spread, the mistakes decreased with increasing field size, but there was a discrepancy in the errors after a 10MV was reached.From the meeting point to the nearest field edge, the field's size decreases to a point where there is a smaller gap, which is related to the amount of secondary electrons at the medium's departure, especially after the LED has emerged. There is a significant drop in the phantom's total dose until the field area gets incredibly small.

It is easy to predict changes in the relative dose percentages for field sizes of 5x5 cm and 10x10 cm, as shown in figures 19 and 20, because the two graphs are quite close to one another regardless of the intensity of the irradiated beam. However, in terms of anticipating the percentages of the dosages, the 3x3 cm field size is rather far from the other field sizes that differ significantly. After this, it becomes difficult to make a meaningful comparison when field sizes smaller than 3x3 cm are used.

4.5 Lung Radiotherapy

Lung cancer treatment and management require radiotherapy; this depends on the previously mentioned criteria, such as the medium's density, field sizes, and beam energy from which the beam energy is transferred. As evidenced by its impacts on the diameters of the field, the LED, and the secondary electrons that flow between the medium, lung density is specifically thought to be a critical influence.Lung density is regulated by an individual's age and health, and as a result, it often varies between 0.1 to 0.4 g/cm3, which is why it is called heterogeneous density even though it is still less than the density of water. Before resorting to a lung radiotherapy present in a low-density medium, it is thought to be important to take into account all the parameters that are responsible for the LED energy and field sizes. Based on a few additional criteria, the results of this experiment will help one make decisions regarding the magnitude of the field provided for a given medium density and a particular beam energy.These elements include an individual's health, characteristics that affect how radiotherapy works, and prior exposures that affect dosage and, in turn, control beam energy and field sizes when lung density is determined.

As the beam energy increases, the LED effect increases. For instance, the 6MV and 10MV with field sizes of 10x10 cm clearly demonstrate the effect of LEDs even at lung densities as low as 0.1 g/cm3. For lung densities of 0.2 g/cm3, 0.3 g/cm3, and 0.4 g/cm3, a 6MV for a field size of 5x5 cm is suggested.It has been shown that a lung density of 0.1 g/cm3 may ultimately result in decreased absorption of the dose present in the lung medium, thereby interfering with the absorption of the required dosage for the treatment of lung cancer. Figure 6 makes it clear that at the point depth of 15 cm and the end of the lung medium, the relative dose absorption percentage is as low as 47%.

Since the relative percentage dose submerged at the end of the lung medium might be about 32%, which is frequently lower for the majority of the radiation in the lungs, a lung density of 0.1 g/cm3 is not thought to be realistic for a beam energy of 6MV with a field size of 3x3 cm. Thus, it has been established that lung densities of 0.2 g/cm3, 0.3 g/cm3, and 0.4 g/cm3 are best suitable for the goal of radiation therapy. The suggested densities are within the range that the American Association of Physicists in Medicine has established. It has also been demonstrated that a field size of 3x3 cm is suitable for inhibiting the development of LEDs and the upper range advancement of secondary electrons.

5. CONCLUSIONS

According to the study's findings, the dosage absorption determined by the TPS is based on the CCCS method, which, when combined with Monte Carlo calculations, yields an accurate result in the context of heterogeneous media and low-density materials like the lungs. The development of the LED and a greater range of secondary

electrons at the end of the lung medium occur for the higher beam energy of the 10MV and the smaller field size of 3x3 cm. The additional ionization is the cause of the ionization chamber curve being higher than the other curve for the 10MV at field size 3x3 cm and density of 0.3 g/cm3. The dose distribution is affected by the lung medium's density and the energy delivered by the beam. In general, as depth increases, dosage absorption decreases. As the beam energy increases, the penumbra breadth grows while the medium density drops. At 10MV, the LED effect increases, a secondary electron is present, and the penumbra's width widens. 6MV is thought to be the most advised energy for the beam because of this. When the field size is 4x4 cm and the beam energy is 8MV, which is used to calculate the CCCS, LED, and secondary electrons using the Monte Carlo Calculation at different densities, more work is required to control the dosage absorption.

REFERENCES

1. Australian Cancer Research Foundation. How radiation is used to treat lung cancer (2021).
2. Sholih, Mally G., et al. "Knowledge, attitudes, and practices of lung cancer risk factors in West Bandung Society." Journal of Pharmacy AndBioallied Sciences 11.8 (2019): 574.
3. Parashar, Bhupesh, Shruthi Arora, and A. Gabriella Wernicke. "Radiation therapy for early stage lung cancer." Seminars in interventional radiology. Vol. 30. No. 02. Thieme Medical Publishers, 2013.
4. Australian Institute of Health and Welfare & Cancer Australia 2011. Lung cancer in Australia: an overview. Cancer series no. 64. Cat. no. CAN 58. Canberra: AIHW.
5. Sholih, Mally Ghinan, et al. "Risk factors of lung cancer in Indonesia: A qualitative study." J. Adv. Pharm. Educ. Res| Apr-Jun 9.2 (2019): 41-45.
6. Samet, Jonathan M., et al. "Lung cancer in never smokers: clinical epidemiology and environmental risk factors." Clinical cancer research 15.18 (2009): 5626-5645.
7. Uzel, Esengül Koçak, Metin Figen, and Ömer Uzel. "Radiotherapy in lung cancer: current and future role." SisliEtfalHastan Tip Bul 53.4 (2019): 353-60.
8. Rachtan, Jadwiga. "Alcoholic beverages consumption and lung cancer cell types among women in Poland." Lung Cancer 35.2 (2002): 119-127.
9. Baumann, Pia, et al. "Outcome in a prospective phase II trial of medically inoperable stage I non–small-cell lung cancer patients treated with stereotactic body radiotherapy." Journal of Clinical Oncology 27.20 (2009): 3290-3296.
10. Vinod, Shalini K., and Eric Hau. "Radiotherapy treatment for lung cancer: Current status and future directions." Respirology 25 (2020): 61-71.
11. Baker, S., Dahele, M., Lagerwaard, F. J., & Senan, S. (2016). A critical review of recent developments in radiotherapy for non-small cell lung cancer. Radiation oncology, 11, 1-14.
12. Alhassani, Ali, Amitabh Chandra, and Michael E. Chernew. "The Sources of the SGR “Hole”." (2012).
13. Mackie, T. R., J. W. Scrimger, and J. J. Battista. "A convolution method of calculating dose for 15-MV x rays." Medical physics 12.2 (1985): 188-196.
14. Estrada Espinosa, Julio Cesar, Segundo Agustín Martínez Ovalle, and Cinthia Kotzian Pereira Benavides. "Dosimetric algorithm to reproduce isodose curves obtained from a LINAC." Computational and Mathematical Methods in Medicine 2014 (2014).
15. Dawod, Tamer. "Evaluation of collapsed cone convolution superposition (CCCS) algorithms in prowess treatment planning system for calculating symmetric and asymmetric field size." Int J Cancer Ther Oncol 3.2 (2015): 8.
16. Calvo, Oscar I., et al. "On the quantification of the dosimetric accuracy of collapsed cone convolution superposition (CCCS) algorithm for small lung volumes using IMRT." Journal of applied clinical medical physics 13.3 (2012): 43-59.
17. El Shahat, K., El Saeid, A., Attalla, E., & Yassin, A. (2014). Comparative Study between Measurement Data and Treatment Planning System (TPS) in Small Fields for High Energy Photon Beams. International Scholarly Research Notices, 2014.